A simulation of electromigration-induced transgranular slits

Weiqing Wang and Z. Suo[a)]
Mechanical and Environmental Engineering Department, Materials Department, University of California, Santa Barbara, California 93106

T.-H. Hao
China Textile University, Shanghai 200051, Peoples Republic of China

(Received 31 July 1995; accepted for publication 3 November 1995)

An on-chip aluminum interconnect carries an intense electric current at an elevated temperature, motivating atoms to diffuse in the solid state, and inducing voids that may cause an open failure. Recent observations have shown that a void sometimes collapses to a slit running nearly perpendicular to the electric current direction. Such a slit often lies inside a grain rather than along a grain boundary. An earlier calculation showed that diffusion on the void surface, driven by the electric current, can cause a circular void to translate in an infinite, isotropic interconnect. It was suggested recently that this solution may be unstable, and that two forces compete in determining the void stability: surface tension favors a rounded void, and the electric current favors a slit. A linear perturbation analysis, surprisingly, revealed that the translating circular void is *stable* against infinitesimal shape perturbation. Consequently, the slit instability must have resulted from finite imperfections. This article reviews the experimental and theoretical findings, and describes a numerical simulation of finite void shape change. We determine the electric field by a conformal mapping of complex variables, and update the void shape for a time step by a variational method. The simulation shows that a finite void shape imperfection or surface tension anisotropy can cause a void to collapse to a slit. © *1996 American Institute of Physics.* [S0021-8979(96)00504-0]

I. INTRODUCTION

Aluminum interconnects in integrated circuits are less than 1 μm wide and about 0.5 μm thick. They carry electric current up to 10^{10} A/m^2, and operate near half of aluminum's melting temperature (933 K). As a result of the small dimensions, intense currents, and elevated temperatures, solid-state mass diffusion driven by the electron wind, known as electromigration, poses persistent reliability problems.[1,2]

Figure 1 contrasts a wide and a narrow interconnect. In a wide line, grain boundaries form a continuous network. Diffusion on grain boundaries is orders of magnitude faster than diffusion in lattice, so that the latter is negligible. Atoms diffuse along the grain boundaries, and voids nucleate and grow. By contrast, a narrow line often has a bamboolike grain structure, where grain boundaries are far apart and nearly perpendicular to the line direction. In addition to rounded voids, slits have been observed both in bamboolike and single-crystalline interconnects.[3–5] A void often nucleates at a junction of grain boundaries, or a junction of a grain boundary and an aluminum passivation interface.[6] The void may enlarge, migrate in a grain, penetrate grain boundaries, change shape, collapse to a slit, and finally sever the interconnect.[7–10] The slit is often found inside a grain instead of along a grain boundary.[9–11] An interconnect is a complex dynamical system that has multiple thermodynamic forces and dissipative processes. It is therefore not surprising that voids in reality do not obey any simple rules, or follow the same sequence of events mentioned here.[7]

Complexity notwithstanding, theoretical analyses have focused on elementary processes in the void dynamics. Void nucleation and growth have been studied by many investigators.[12–15] Void migration is understood in terms of surface diffusion.[16,17] Atoms diffuse on the void surface from one portion of the void to another, so that the void appears to translate in the grain. It has been suggested that a rounded void is unstable: the electric current may amplify a small asymmetry in the void shape and cause the void to collapse to a slit.[9,10] Two forces compete in determining the void shape. Surface tension favors a rounded void, and the electric current favors a slit; a rounded void collapses to a slit when the electric current prevails.[18,19] A linear stability analysis, however, shows that a circular void translating in an infinite, isotropic conductor is stable against any infinitesimal shape perturbation.[20] Consequently, a slit may result from a finite shape imperfection. Indeed, recent simulations show that a circular void in an interconnect of finite width is unstable and evolves to a slit.[21,37]

In an interconnect with the bamboolike grain structure, grain boundaries no longer serve as long-range mass transport paths. Interfaces between aluminum and surrounding materials may provide a fast diffusion path.[22] Dislocations may also be important: not only do they act as fast diffusion pipes, but they also climb and multiply under electric current.[23] Even lattice diffusion may become significant when no other diffusion paths are available.

In this article, we will simulate void shape change due to surface diffusion, assuming all other transport processes are negligibly slow during shape change. Section II formulates the dynamics of a void in the electron wind. Section III summarizes the existing analytical solution of a translating circular void, and Sec. IV of linear stability analysis. Section V describes a variational method to simulate the large void shape change. The results in Sec. VI show that a finite shape

[a)]Electronic mail: zhigang@engineering.ucsb.edu

 0021-8979/96/79(5)/2394/10/$10.00

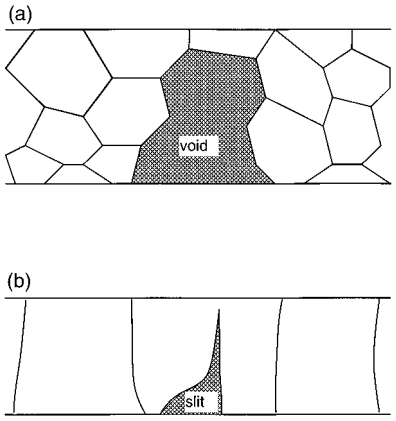

FIG. 1. (a) A rounded void in a wide polycrystal interconnect. (b) A transgranular slit in a narrow interconnect with the bamboolike grain structure.

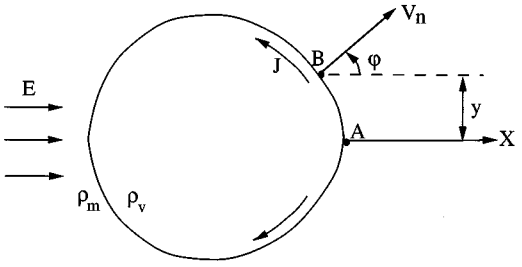

FIG. 2. A void in an interconnect subjected to an electric field. The medium inside the void may have finite resistivity.

imperfection or a surface tension anisotropy may destabilize a void. Table I lists material properties to be used in numerical estimates.

II. THE EVOLVING VOID AS A DYNAMICAL SYSTEM

A. Kinematics, energetics, and kinetics

Figure 2 illustrates a void in a conductor under an electric field E, where the rectangular coordinates x and y are also indicated. We will model a cylindrical void through the thickness of the conductor. The void changes location and shape by mass diffusion on the void surface. The void is a dynamical system, and the mathematical problem is to evolve a closed contour in a plane.

Following the classical differential geometry,[24] we describe the contour at a given time t by the position vector $\mathbf{x}$ as a function of a parameter θ, namely,

$$\mathbf{x}=\mathbf{x}(\theta,t). \tag{2.1}$$

For example, $x=a\cos\theta$ and $y=b\sin\theta$, $0<\theta<2\pi$, describe an ellipse, with a and b evolving with the time. At a given time, one can calculate the length of an arc element ds, the vector normal to the arc element $\mathbf{n}$, and the curvature of the arc element κ. A sign convention is adopted such that $\mathbf{n}$ points from the void to the solid, and $\kappa>0$ for a circular void.

Denote the velocity normal to the surface by V_n (i.e., the volume of mass removed from unit surface area in unit time). The velocity relates to position vector on the void perimeter as

$$V_n=\mathbf{n}\cdot\frac{\partial\mathbf{x}}{\partial t}=\frac{\partial y}{\partial s}\frac{\partial x}{\partial t}-\frac{\partial x}{\partial s}\frac{\partial y}{\partial t}. \tag{2.2}$$

Let J be the atomic flux on the void surface (i.e., the number of atoms per time crossing unit length on the surface). Mass conservation requires that the surface velocity relate to the *flux divergence*

$$V_n=\Omega\,\partial J/\partial s. \tag{2.3}$$

Here Ω is the volume per atom. Equations (2.1)–(2.3) specify the kinematics of the dynamical system. (In a continuum model, an atom is a unit for mass, which does not imply discreteness.)

The electron wind exerts a force on an atom on the void surface, F_E, in the direction of the electron flow, of magnitude proportional to the electric field. Let E_t be the component of the electric field tangential to the void surface. The electron wind force per atom is written as[1,2]

$$F_E=-Z^*eE_t, \tag{2.4}$$

where $Z^*(>0)$ is the effective valence, and e (>0) the magnitude of the electron charge. The negative sign means that the force is in the direction of the electron flow.

Let G be the free energy, consisting of surface energy and electrostatic energy—they both vary when the void changes shape. The relative magnitude of the two energies is described by a dimensionless number $\epsilon E^2R_0/\gamma$, where R_0 is the length representative of the void size, γ the surface tension, and ϵ the permittivity. For typical values, this number is much smaller than unity. Consequently, we will take the free energy to be the surface energy, and ignore the electrostatic energy. Thus, the free energy of the system is

$$G=\int\gamma ds. \tag{2.5}$$

All integrals in this article extend over the void surface. The surface tension γ may depend on crystalline orientation.

Following a previous article[25] we will define the thermodynamic force using *virtual motion*. Imagine that the void changes shape slightly, mass relocating from one segment of the surface to another. Denote the small movement normal to the void surface by δU_n; the magnitude of the movement need not be the same along the surface. Let δI be the number of atoms across unit length on the surface. Following Biot,[27] we will call I the mass displacement. Mass conservation requires that δU_n and δI satisfy a relation like (2.3), i.e.,

TABLE I. Pure aluminum data.

Atomic volume	$\Omega=1.66\times10^{-29}$ m^3
Surface diffusivity	$D_s=10^{-5}\times\exp[-0.7(\mathrm{eV})/kT]$ m^2/s [36]
Effect surface thickness	$\delta_s=2.86\times10^{-10}$ m (approximated by the Burgers vector)
Surface energy	$\gamma=1$ J/m^2
Effective valence	$Z^*=20$
Electric resistivity	$\rho=2.74\times10^{-8}\ \Omega$ m

$\delta U_n = \Omega \partial(\delta I)/\partial s$. A small, mass-conserving motion is a virtual motion, so called because it need not obey any kinetic law.

Associated with this virtual motion, the free energy changes by δG, and the electron wind force does virtual work, $\int F_E \delta I ds$. Define the thermodynamic force that drives atomic diffusion on the void surface, F, as free energy reduction plus the virtual work done by the electron wind, associated with one atom moving unit distance. That is, for any virtual motion, F satisfies

$$\int F \delta I ds = -\delta G + \int F_E \delta I ds. \tag{2.6}$$

This definition is consistent with that of Herring[26] on the basis of the chemical potential, as shown in Sec. III A, and will lead to a numerical procedure presented in Sec. V. Equations (2.4)–(2.6) specify the energetics of the dynamical system.

We will adopt a commonly used linear kinetic law, i.e., the *actual flux* is proportional to the thermodynamic force, namely,

$$J = MF, \tag{2.7}$$

where M is the atomic mobility on the void surface, which we regard as a phenomenological quantity to be determined experimentally by its macroscopic consequences. This linear law is often a good approximation because the potential drop, over an atomic spacing b, is much smaller than the average thermal energy kT, namely, $Fb/kT \ll 1$. The mobility is related to the effective surface diffusivity, $D_s \delta_s$, by the Einstein relation $M = D_s \delta_s / \Omega kT$. Equation (2.7) specifies the kinetics of the dynamical system.

The above completes the problem description. As with many continuum descriptions of natural phenomena, this description can be cast into two forms. They are mathematically equivalent, but lead to different computational schemes. In the first form, a combination of Eq. (2.6) and mass conservation gives an expression of the thermodynamic force F in terms of local quantities (curvature and surface tension), leading to a high-order partial differential equation to be solved analytically or numerically by the finite difference method. In the second form, a combination of Eqs. (2.6) and (2.7) gives an integral representation of the problem, with mass conservation as a constraint, providing the basis for the Galerkin method or the finite element method. We will use both forms in this article to our advantage.

B. Electric field around a void

To determine the electron wind force requires that the electric field be solved for a given void shape. We assume that the electric field distribution is unaffected by electromigration and capillarity, and obeys the standard equations summarized below. The electric field components, E_x and E_y, are the gradients of the electric potential ϕ

$$E_x = -\partial\phi/\partial x, \quad E_y = -\partial\phi/\partial y. \tag{2.8}$$

Conservation of electric charge requires that the components of the current density vector, j_x and j_y, satisfy

$$\frac{\partial j_x}{\partial x} + \frac{\partial j_y}{\partial y} = 0. \tag{2.9}$$

The electric field and the current density relate linearly

$$E_x = \rho j_x, \quad E_y = \rho j_y, \tag{2.10}$$

where ρ is the resistivity. A combination of Eqs. (2.8)–(2.10) shows that the electric potential obeys the Laplace Eq.

$$\frac{\partial^2 \phi}{\partial x^2} + \frac{\partial^2 \phi}{\partial y^2} = 0. \tag{2.11}$$

This partial differential equation, together with boundary conditions, determines the electric potential. The electric field component tangential to the void perimeter is calculated from the gradient of the electric potential in the direction of the arc length

$$E_t = -\partial\phi/\partial s. \tag{2.12}$$

Since there might be conductive species trapped in the void, we assume different resistivity inside the void, ρ_v, and outside the void, ρ_m. If the void is a perfect insulator, $\rho_v = \infty$. A list of useful solutions follows:

A circular void lies in an infinite interconnect.

In this case, the electric field is nonuniform outside the void, but uniform inside the void. Denote the electric field inside the void by E_{void}, which points in the same direction as the remotely applied electric field E, and has magnitude

$$E_{\text{void}} = \alpha E, \tag{2.13}$$

with $\alpha = 2\rho_v/(\rho_v + \rho_m)$. The coefficient varies within a factor of 2 for all reasonable situations, $1 < \rho_v/\rho_m < \infty$.

The medium inside the void has the same resistivity as the conductor, $\rho_v/\rho_m = 1$.

In this case the electric field is uniform everywhere, and the electric potential is

$$\phi = -Ex. \tag{2.14}$$

This solution applies to a void of arbitrary shape in an interconnect of any width. As will be shown later, even this trivial field distribution gives rise to interesting void dynamics.

An insulating void lies in an infinite interconnect, $\rho_v/\rho_m = \infty$.

The solution is readily obtained by complex variable methods; the formulas to be used later are (2.18) and (2.20). Define a complex variable $z = x + iy$, where $i = \sqrt{-1}$. Let $\omega(z)$ be an arbitrary analytic function. The general solution of the Laplace Eq. is

$$\phi = \text{Re}[\omega], \tag{2.15}$$

where Re stands for the real part of a complex number. The electric current flowing across a curved segment AB is given by

$$\int_A^B j_n ds = -\frac{1}{\rho} \text{Im}[\omega], \tag{2.16}$$

where Im stands for the imaginary part of a complex number.

Next consider another complex plane, the ζ-plane, and a unit circle on the plane, $\zeta = \exp(i\theta)$, $0 < \theta < 2\pi$. A power series

$$z = a_{-1}\zeta + a_0 + \sum_{n=1}^{\infty} a_n \zeta^{-n} \tag{2.17}$$

maps the exterior of the unit circle on the ζ plane to the exterior of the void on the z plane. The coefficients a_i describe the shape of the void on the z plane. For example, a_{-1} describes a circle, and a_0 a shape-preserving translation. During void shape evolution, the unit circle on the ζ plane remains unchanged, and the coefficients a_i evolve with the time.

We will assume that the void shape has a mirror symmetry with respect to the x axis, so that all the coefficients a_i are real numbers. This situation also models a void at the surface of a semi-infinite interconnect. Written in real numbers, a point on the unit circle at angle θ maps to a point on the void perimeter, (x,y), according to

$$\begin{cases} x = a_{-1} \cos\theta + a_0 + \sum_{n=1}^{\infty} a_n \cos n\theta \\ y = a_{-1} \sin\theta - \sum_{n=1}^{\infty} a_n \sin n\theta. \end{cases} \tag{2.18}$$

The analytic function ω is determined by the boundary conditions: the electric field is E as $|z|\to\infty$, and the current density normal to the void perimeter, j_n, vanishes. That is, $\omega \to -Ez$ as $|z|\to\infty$ and, according to Eq. (2.16), $\mathrm{Im}[\omega]=0$ on the void surface. Thus,

$$\omega = -a_{-1}E(\zeta + \zeta^{-1}). \tag{2.19}$$

Consequently, the electric potential on the void surface is

$$\phi = -2a_{-1}E \cos\theta. \tag{2.20}$$

This solution is valid for an insulating void, symmetric about the x axis, in an infinite interconnect, subject to the electric field E in the x direction.

III. A VOID IN AN ISOTROPIC CONDUCTOR

This section summarizes analytical results for a void in a conductor that has isotropic surface tension, surface mobility, and effective charge. The results will guide later simulations.

A. Length scale, time scale, and equation of motion

When the surface tension is isotropic, Herring[26] showed that

$$\delta G = \gamma \int \kappa \delta U_n ds. \tag{3.1}$$

The integral is the increase in the length of the void perimeter associated with the virtual motion. Inserting this expression into Eq. (2.6), using the mass conservation relation $\delta U_n = \Omega \partial(\delta I)/\partial s$, and integrating by parts, one obtains the thermodynamic force

$$F = -Z^* e E_t + \Omega\gamma \partial\kappa/\partial s. \tag{3.2}$$

The first term is the electron wind force; the second term is the capillary force, which reproduces Herring's formula.

With reference to Fig. 2, consider the shape evolution of an initially circular void of radius R_0. The relative magnitude of the two forces, the electron wind and the surface tension, is measured by a dimensionless group[18,19]

$$\chi = \frac{Z^* e E R_0^2}{\Omega\gamma}. \tag{3.3}$$

This number is of primary importance and will appear many times later. Note that the length scale R_0 enters this group; its physical significance will become evident when we consider void instability.

We will normalize all the lengths by the radius of the circular void, R_0, and normalize the electric field in the conductor by the remotely applied electric field E. The combination of the equations in Sec. II A suggests a characteristic time

$$t_0 = \frac{R_0^4}{\Omega^2 M \gamma}. \tag{3.4}$$

All the time in this article will be reported in this characteristic unit.

Combining the equations in Sec. II A, we obtain the *equation of motion* for the dynamical system

$$\mathbf{n}\cdot\frac{\partial \mathbf{x}}{\partial t} = \frac{\partial^2}{\partial s^2}(\chi\phi + \kappa). \tag{3.5}$$

This is a partial differential equation in a dimensionless form, valid when the conductor has isotropic surface tension, surface mobility, and effective charge.

B. A shape-preserving circular void translates in an infinite conductor

Ho[13] discovered many years ago that, in an infinite, isotropic conductor under a remote uniform electric field, a circular void can migrate without changing its shape. His solution is summarized as follows, and will be used to guide the later development. For a circular void of radius R_0, from Eq. (2.13), one obtains the electric field component tangential to the void surface, $E_t = -\alpha E y/R_0$, so that the electron wind force [see Eq. (2.4)] is

$$F_E = \alpha e Z^* E y/R_0. \tag{3.6}$$

The isotropic surface tension does not cause diffusion on the surface of the circular void.

On the void surface in Fig. 2, A is a symmetry point where the flux vanishes, and B is a point at height y. Let the circle translate at a uniform velocity V in the x direction. In unit time, atoms of volume yV are removed from the segment AB, and flow out of the segment at point B. Mass conservation requires that the flux at point B be

$$J = yV/\Omega. \tag{3.7}$$

A combination of Eqs. (2.7), (3.6), and (3.7) gives the steady-state velocity

$$V = \alpha\Omega M Z^* e E/R_0. \tag{3.8}$$

The void migrates in the direction of the applied electric field, at a velocity proportional to the applied electric field,

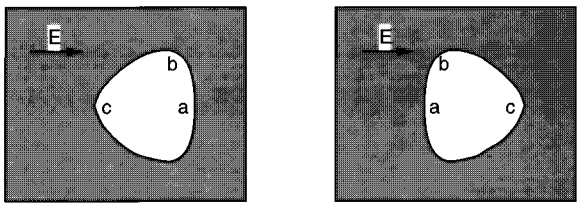

(a) "critical" (b)"uncritical"

FIG. 3. (a) A void with the critical asymmetric shape. (b) A void with the uncritical asymmetric shape. Adapted from Arzt, *et al.*[10] (see Ref. 10).

and inversely proportional to the void radius. At $T=500$ K and $E=1000$ V/m an insulating void of radius $R_0=0.1$ μm translates at velocity $V=2.4\times10^{-9}$ m/s.

C. Intense electron wind blows a void away from a trap

A void is subject not only to the electron wind, but also to the forces like grain-boundary tension. In a bamboolike interconnect, grain boundaries or junctions may trap voids. A critical electric field exists, above which the void breaks away from the trap.[22] Following similar analyses for a precipitate[28] and a dislocation loop,[23] we estimate the critical electric field for a void using the principle of virtual work.

Denote f_T as the force by the trap applied to the void. For example, when a void tries to break away from a grain boundary of tension γ_b, the grain boundary exerts a force (per interconnect thickness) on the void, $f_T=2\gamma_b$, in the direction opposing the breakaway. In equilibrium this force balances the electron wind force, and surface diffusion stops. Let the void undergo a virtual translation in the x direction by a displacement δU. The associated virtual mass displacement, δI, satisfies a relation similar to Eq. (3.7), i.e., $\delta I = y\,\delta U/\Omega$. In equilibrium, the total virtual work vanishes

$$\int F_E \delta I ds - f_T \delta U = 0. \tag{3.9}$$

Inserting Eq. (3.6) and approximating the void by a circle in integration, we obtain that

$$\frac{\alpha Z^* e E R_0^2}{\Omega f_T} = \frac{1}{\pi}. \tag{3.10}$$

Material properties being fixed, a critical value of ER_0^2 exists, above which the void breaks away from the grain boundary. Taking $\gamma_b=0.5$ J/m^2 and $\alpha=2$, we find that a void of $R_0=0.1$ μm breaks away from the grain boundary under $E=82.5$ V/m.

IV. LINEAR STABILITY ANALYSIS

A translating circular void is a solution, but may be unstable. Arzt and co-workers[9,10] suggested that the electron wind may amplify certain perturbation from the circular shape, leading to a slit. Figure 3 illustrates two asymmetric void shapes. The shape in Fig. 3(a) is critical because the electromigration-induced atomic flux from b to c is larger than that from a to b, so that mass depletes from b, and the void elongates normal to the interconnect line direction. By contrast, the shape in Fig. 3(b) is uncritical because the electromigration-induced atomic flux from c to b is larger than that from b to a, so that mass accumulates at b, and the void elongates along the interconnect line direction.

Two forces, the electron wind and the surface tension, compete in determining the shape stability.[18,19] The former destabilizes a circular void, and the latter stabilizes it. The relative magnitude of the two forces is measured by the dimensionless group χ of Eq. (3.3). When χ is small, the surface energy dominates, and the void remains rounded. When χ is large, the electron wind dominates, and void collapses to a slit.

Marder's linear stability analyses,[20] however, do *not* completely support the above qualitative picture. He prescribed infinitesimal perturbation to the translating circular void in an infinite, isotropic interconnect carrying an electric current, and found the following results. If $\rho_v/\rho_m=1$ the void is unstable when χ exceeds a critical value. An insulating void ($\rho_v/\rho_m=\infty$), however, is stable for arbitrarily high χ. Hao[29] extended the analysis and showed that a void with finite resistivity is unstable when χ exceeds a critical value that depends on ρ_v/ρ_m. The remainder of this section casts Marder's results in the notation of this article.

The translating circular void in Sec. III B is described by

$$a_{-1}=1, \quad a_0=\alpha\chi t, \tag{4.1}$$

with all other coefficients vanishing. One can confirm that Eq. (4.1) is a solution to the partial differential Eq. (3.5). We next impose a small perturbation as

$$a_{-1}=1+\epsilon_{-1}, \quad a_0=\alpha\chi t+\epsilon_0. \tag{4.2}$$

In addition, all other coefficients, $a_1, a_2 ...$, perturb from zero.

A. If $\rho_v/\rho_m=1$, the void is unstable when χ exceeds a critical value

In this case the dimensionless electric potential is simply $\phi=x$. Substituting the perturbed coefficients into Eq. (3.5) and keeping the first-order terms, one obtains that

$$\begin{cases} \dot{\epsilon}_{-1}=0 \\ \dot{\epsilon}_0=-\chi\epsilon_{-1}+\dfrac{3}{2}\chi a_1 \\ \dot{a}_n=\chi\dfrac{n^2-1}{2}a_{n-1}-n(n+2)(n+1)^2 a_n+\chi\dfrac{(n+1)(n+3)}{2}a_{n+1} \quad (n\geqslant 1) \end{cases} \tag{4.3}$$

TABLE II. Eigenvalues of the ordinary differential equations ($\rho_v/\rho_m=1$, $N=10$).

$\chi=10$	$\chi=11$
−1.48	+0.84
−66.46	−62.96
−232.96	−231.50
−593.22	−591.81
−1253.37	−1251.99
−2345.47	−2344.10
−4025.53	−4024.18
−6473.58	−6472.24
−9894.15	−9893.07
−14 583.74	−14 597.00

The superimposed dots indicate time derivatives.

This is a set of linear ordinary differential equations. The solution can be a superposition of two solutions with different initial conditions

$$\text{I.}\quad \epsilon_{-1}(0)\neq 0,\quad \epsilon_0(0)\neq 0;\quad a_1(0)=0,\quad a_2(0)=0\ldots$$

$$\text{II.}\quad \epsilon_{-1}(0)=0,\quad \epsilon_0(0)=0;\quad a_1(0)\neq 0,\quad a_2(0)\neq 0\ldots$$

The solution under initial condition I is

$$\begin{cases} \epsilon_{-1}(t)=\epsilon_{-1}(0) \\ \epsilon_0(t)=\epsilon_0(0)-\chi\epsilon_{-1}t \\ a_n(t)=0. \end{cases} \tag{4.4}$$

This solution is a circular void. Under initial condition II, the solution is determined by the set of equations of the last line in Eq. (4.3). They are solved by the exponential functions

$$a_n(t)=a_n(0)\exp(\lambda t). \tag{4.5}$$

Here $a_n(0)$ describe the initial perturbation from the circular shape, and λ is an eigenvalue of the matrix formed by the coefficients of the equations in (4.3). When $\lambda<0$, the solution decays exponentially, and the circular void is stable. When $\lambda>0$, the solution grows exponentially, and the circular void is unstable.

We used finite number of terms, N, in the calculation; the computed eigenvalues with $N=10$ are listed in Table II. When χ is small, all eigenvalues are negative. When χ is large, some eigenvalues are positive. The critical value is between $10<\chi_c<11$, which agrees with our previous result $\chi_c=10.65$, obtained from a noncircular steady-state solution.[19]

TABLE III. Eigenvalues of the ordinary differential equations ($\rho_v/\rho_m=\infty$, $N=10$).

$\chi=20$	$\chi=200$
−12.00	−12.00
−119.69	−724.58
−316.37	−1519.05−1503.09i
−687.32	−1519.05+1503.09i
−1351.53	−2912.23−5036.97i
−2445.67	−2912.23+5036.97i
−4127.16	−5208.85−11 472.19i
−6572.66	−5208.85+11 472.19i
−10 083.68	−9725.56−23 378.06i
−13 751.91	−9725.56+23 378.06i

B. An insulating void is stable against infinitesimal shape perturbation

In this case, the electric potential is given by Eq. (2.20). The same procedure leads to

$$\begin{cases} \dot{\epsilon}_{-1}=0 \\ \dot{\epsilon}_0=-2\chi\epsilon_{-1}+\chi a_1 \\ \dot{a}_n=\chi(n^2-1)(a_{n-1}-a_{n+1})-n(n+2)(n+1)^2a_n. \end{cases} \tag{4.6}$$

Within the range $N<100$ and $\chi<200$, we found that the real parts of eigenvalues are all negative; Table III gives examples. We stop at $\chi=200$ because this corresponds to an electric field an order of magnitude higher than that used in the accelerated tests. Thus, the insulating void is stable against infinitesimal shape perturbation.

V. NUMERICAL PROCEDURE

Linear stability analysis has two limitations. First, it gives no information about the behavior after the circular void loses stability. Will the void collapse to a slit, or will it settle down with a noncircular shape, translating without further shape change? Second, a void stable against infinitesimal perturbation need not be stable against finite perturbation. In practice, the initial void is never a perfect circle; deviation may result from surface tension anisotropy, finite interconnect width, thermal stress, etc. To determine the void stability under practical conditions, we must study *large shape change*.

In the previous articles,[25,30] we outlined a variational method for the electromigration problem. The method of this kind, pioneered by Needleman and Rice,[31] has been developed by several research groups to simulate diverse phenomena of structural evolution in materials.[30–35] A general formulation of the finite element method for electromigration problems has been given recently.[37] In what follows, we give the details of the method in the context of this work.

A combination of the force definition (2.6) and the kinetic law (2.7) gives

$$\int \frac{J}{M}\,\delta I ds=-\delta G+\int F_E\delta I ds. \tag{5.1}$$

In the previous article,[25] this equation leads to a variational statement. Here we directly apply the Galerkin procedure to this equation. Describe the void shape by a set of generalized coordinates, a_i; they are the coefficients in the power series (2.18) in the present problem. Write $\dot{a}_i$ as the generalized velocities.

The kinematics require that the flux be linear in the generalized velocities

$$J=\sum_k A_k\dot{a}_k. \tag{5.2}$$

Here A_i are analogous to the shape functions in finite element methods. They are computed as follows. In a dimensionless form, the mass conservation Eq. (2.3) is

$$\frac{\partial J}{\partial s}=\left(\frac{\partial y}{\partial \theta}\frac{\partial x}{\partial t}-\frac{\partial x}{\partial \theta}\frac{\partial y}{\partial t}\right)\frac{d\theta}{ds}. \tag{5.3}$$

The quantities in the bracket relate to the generalized coordinates and velocities by Eq. (2.18). Integrating and taking $J=0$ at $\theta=0$, we obtain the flux $J(\theta)$ in the form (5.2), with the shape functions given by

$$A_{-1}=a_{-1}\theta-\sum_{n=1} a_n \frac{n\,\sin(n+1)\theta}{n+1}, \tag{5.4a}$$

$$A_0=a_{-1}\,\sin\,\theta-\sum_{n=1} a_n \sin\, n\theta, \tag{5.4b}$$

$$A_k=a_{-1}\frac{\sin(k+1)\theta}{k+1}-ka_k\theta - \sum_{\substack{n=1\\ n\neq k}} na_n \frac{\sin(k-n)\theta}{k-n}, \quad (k=1,2,\ldots). \tag{5.4c}$$

Since no net mass is added or removed from the void, the flux $J(\theta)$ should be a periodic function with period 2π. In the above, only the function θ is aperiodic. Consequently, mass conservation places a constraint among the coefficients

$$a_{-1}\dot{a}_{-1}-\sum_{k=1} ka_k\dot{a}_k=0. \tag{5.5}$$

One can confirm that this constraint ensures that the cross-section area of the cylindrical void remains constant as the shape changes. We used a Lagrange multiplier to incorporate the constraint into the numerical simulation.

The same kinematics require that the virtual mass displacement be linear in the virtual coordinate change

$$\delta I=\sum_i A_i\delta a_i. \tag{5.6}$$

The shape functions are the same as Eq. (5.4).

Insert Eqs. (5.2) and (5.6) into Eq. (5.1), and we obtain

$$\sum_{i,k} H_{ik}\dot{a}_k\delta a_i=\sum_i (f_i+f_{Ei})\delta a_i. \tag{5.7}$$

Each term in Eq. (5.7) has a clear physical meaning. The free energy depends on the void shape, and is therefore a function of the coordinates, $G(a_{-1},a_0,a_1,a_2,\ldots)$. The generalized force column resulting from the free energy is

$$f_i=-\partial G/\partial a_i. \tag{5.8}$$

The generalized force column resulting from the electron wind is

$$f_{Ei}=\int F_E A_i ds. \tag{5.9}$$

The generalized viscosity matrix is

$$H_{ik}=\int \frac{A_iA_k}{M}\,ds. \tag{5.10}$$

The viscosity matrix is symmetric and positive–definite. The above integrals are evaluated numerically when necessary.

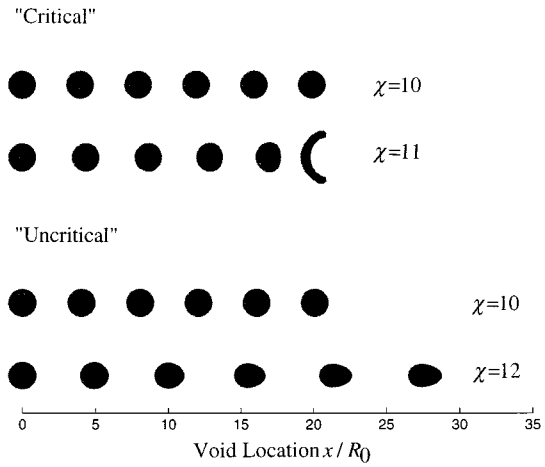

FIG. 4. Each row is a sequence of snapshots, taken at time interval $\Delta t=0.4$, of a void migrating in an interconnect, in the direction of the applied electric field, from the left to the right. The electric resistivities inside and outside of the void are identical, $\rho_v/\rho_m=1$. The initial perturbation is $\epsilon=0.01$.

Equation (5.7) holds for any arbitrary virtual motion, so that

$$\sum_k H_{ik}\dot{a}_k=f_i+f_{Ei}. \tag{5.11}$$

That is, the viscosity times the velocity equals the force. This is a set of ordinary equations that evolve the generalized coordinates. We use a standard computer routine to integrate the equations numerically.

VI. SIMULATION RESULTS

The following results are computed with $N=15$ coordinates. We run the simulation with a perfect circular void under electric field up to $\chi=200$, for both cases $\rho_v/\rho_m=1$ and $\rho_v/\rho_m=\infty$. The voids are found to translate at a steady-state velocity as determined by Eq. (3.8). This shows that round-off error of the machine is small enough not to change the stability of the void, even in the case where the void is linearly unstable.

A. Case $\rho_v/\rho_m=1$

The initial imperfect circle may take any shape. To be definite, we prescribe the initial void shape as

$$a_{-1}=\sqrt{1+\epsilon^2},\quad a_1=\pm\epsilon,\quad a_i=0\quad (i\neq\pm 1). \tag{6.1}$$

The parameter ϵ indicates the magnitude of the imperfection, and a_{-1} is chosen so that the noncircular void has the same area as a unit circle. The two signs of a_1 give two asymmetries in Fig. 3. Figure 4 shows the results of the simulation ($\epsilon=0.01$). Each row is a sequence of snapshots of a void for a level of χ, taken at time interval $\Delta t=0.4$. The void migrates in the direction of electric current, from the left to the right; the location of the void can be read from the ruler. For the critical asymmetry, $a_1=-0.01$, once the void buckles, it collapses to a slit. Figure 5 details the slit formation in the case $\chi=11$, where only half of the void is drawn because of the symmetry. The time is mostly spent on the initial shape change from the circle, and the later stage of slit formation is

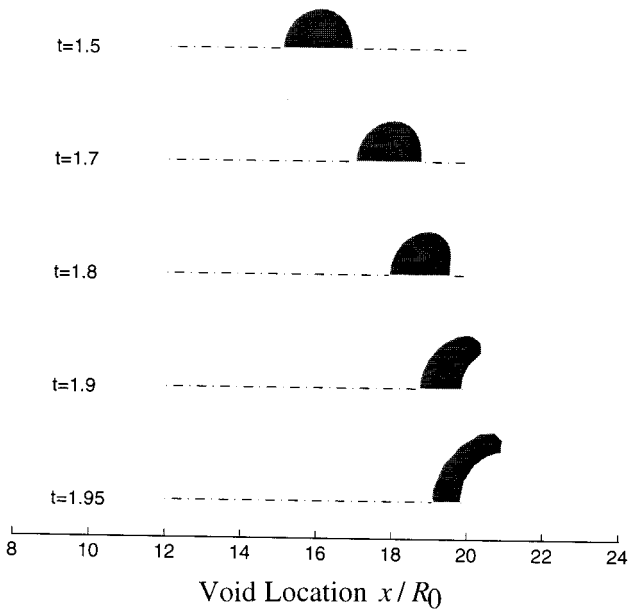

FIG. 5. Details of the late stage void evolution of the critical situation for $\chi=11$ in Fig. 4.

fast. Because the void is linearly unstable, the critical value χ_c is insensitive to the initial perturbation, so long as the perturbation is small. The value computed with $\epsilon=-0.001$ is between $10<\chi_c<11$, in agreement with the linear stability analysis in the last section.

For the uncritical asymmetry, $a_1=+0.01$, after the circle loses stability, the void reaches an egg-shaped steady state, translating without further shape change. If the electric field increases, the void elongates more, until the upper and the lower part of the void surface touch. The void might then split into two smaller ones.

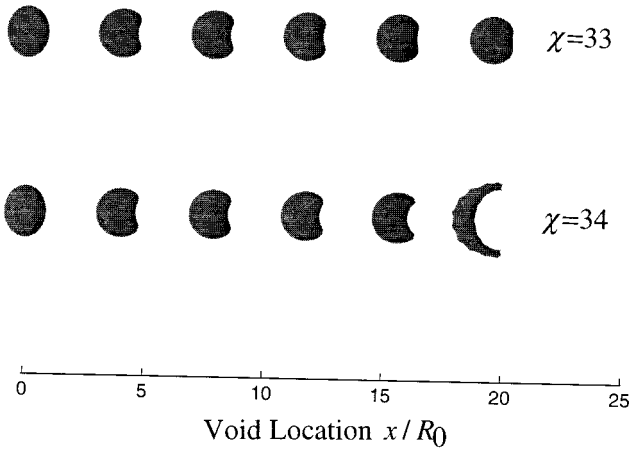

FIG. 6. Each row is a sequence of snapshots, taken at time interval $\Delta t=0.06$, of a void migrating in an interconnect, in the direction of the applied electric field, from the left to the right. The void is a perfect insulator. The initial perturbation is $\epsilon=0.1$.

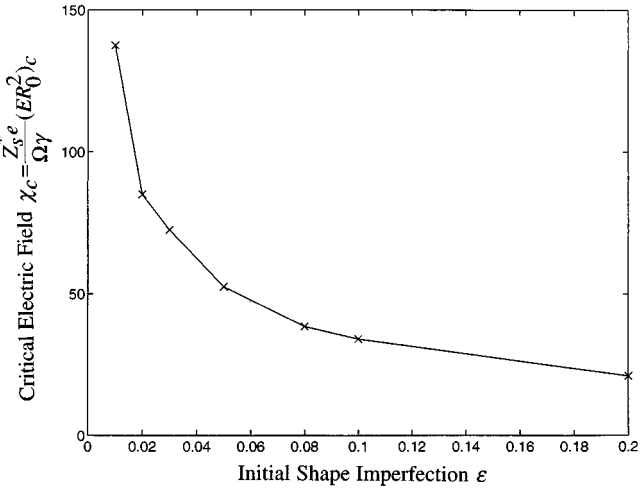

FIG. 7. The critical value χ_c as a function of the magnitude of the initial shape imperfection ϵ.

B. Case $\rho_v/\rho_m=\infty$

As discussed in Sec. IV B, an insulating void, in an infinite, isotropic interconnect, with infinitesimal perturbation, will relax back to a circle. Our simulation, detailed as follows, shows that the insulating void is unstable against finite imperfection. We will still present our results in terms of the dimensionless group χ in Eq. (3.3). The critical value for a rounded void to evolve to a slit, χ_c, now depends on the type and the magnitude of the imperfection. The imperfection may be introduced in many ways, such as finite resistivity inside the void,[29] finite interconnect width,[21,37] as mentioned before. Three other types of imperfections are considered as follows.

1. Finite shape imperfection

In the simulation, the void takes the initial shape of Eq. (6.1). Figure 6 shows the snapshots at time interval $\Delta t=0.06$ of a void with initial imperfection $\epsilon=0.1$. When χ is small, the void migrates and changes its shape, but finally reaches a steady state. When χ is large, the void collapses into a slit. Figure 7 plots χ_c as a function of the imperfection ϵ. The critical value drops sharply when moderate initial imperfection is introduced, and decreases somewhat thereafter.

2. Surface energy anisotropy

Consider a film with the plane parallel to (111) plane. The (111) planes are taken to have lower surface tension than other crystalline planes. Under no electron wind, a void is faceted with (111) planes. That is, we assume that the void is approximately a truncated tetrahedron. To explore the effect of the anisotropy on slit instability, we assume that the surface tension is a function of surface orientation. Denote φ as the angle from the x axis to the surface normal vector **n**. In the numerical simulation, the function is taken to have a threefold symmetry

$$\gamma=\gamma_0(1+g_s\cos 3\varphi). \tag{6.2}$$

The magnitude of g_s indicates the degree of anisotropy, and the sign gives two crystal orientations relative to the electric

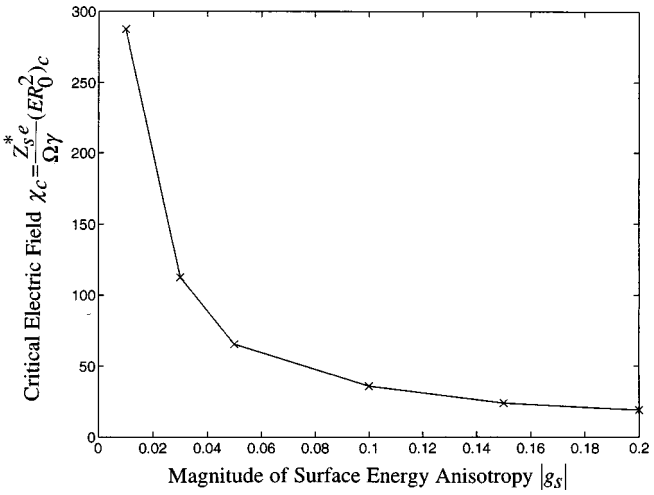

FIG. 8. The critical value χ_c as a function of the magnitude of surface energy anisotropy.

field. The average surface tension γ_0 enters the dimensionless group χ in Eq. (3.3) and the characteristic time in Eq. (3.4). We will still use the two-dimensional electric field developed in Sec. II B; this should give a good approximation when the in-plane void size is large compared to the film thickness.

In the simulation, we start with a circular void, and let it relax under the anisotropic surface tension to the noncircular equilibrium shape. An electric field is then applied and the void migrates and changes shape again. Under the critical configuration ($g_s<0$), for a given g_s, there is a critical electric field χ_c, above which the void collapses to a slit. The void evolution sequence is similar to that of shape imperfection. Figure 8 plots the critical value χ_c as a function of the anisotropy factor g_s. Surface energy anisotropy drastically reduces the critical electric field.

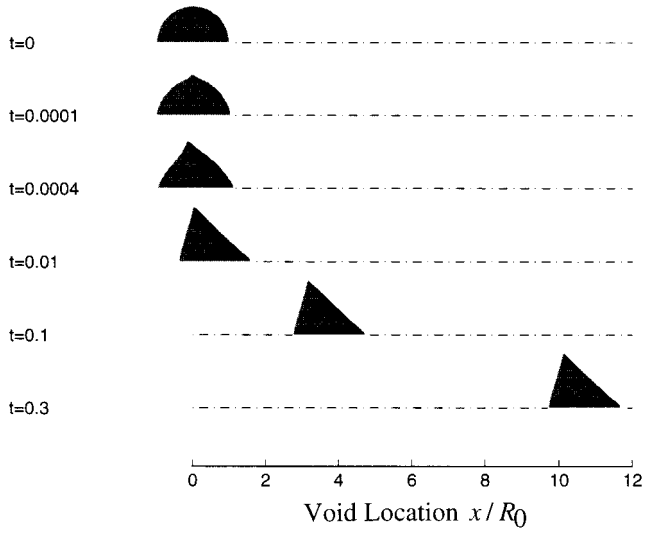

FIG. 9. Void evolution for $\chi=100$ and high surface diffusivity anisotropy $g_d=0.99$.

TABLE IV. Effect of surface diffusivity anisotropy on void stability.

g_d	$g_s=-0.1$	$g_s=0$	$g_s=+0.1$
−0.99	Uncritical	Uncritical	Uncritical
−0.9	Uncritical		Uncritical
−0.1	Uncritical		Uncritical
0.0	$35<\chi_c<37$	Circle	Uncritical
+0.1	$15<\chi_c<16$		$13<\chi_c<14$
+0.9	$29<\chi_c<30$		$240<\chi_c<260$
+0.99	Uncritical	Uncritical	Uncritical

3. Mobility anisotropy

Atomic diffusivity on the void surface can be nonuniform due to, for example, crystalline anisotropy or temperature nonuniformity caused by the Joule heating. The effect of diffusivity anisotropy has been modeled with a sixfold symmetry.[21] Consequently, the void becomes faceted under the electric current, resulting in a hexagonal shape which is stable. In the present simulation, to model the truncated tetrahedron, we adopt the threefold symmetry of form

$$M=M_0(1+g_d\cos 3\varphi). \tag{6.3}$$

The parameter g_d dictates the magnitude and two configurations relative to the electric current. The average mobility M_0 enters the characteristic time (3.4). Figure 9 shows snapshots for a void under $\chi=100$ with anisotropy $|g_d|=0.99$. In this case surface diffusion at some parts of the void surface is about 200 times faster than at other parts. The lowest diffusivity limits the flux, and the void tends to have polygonal shapes. The migration velocity of the void as a whole is limited by the slowest diffusion on the void surface.

The situation complicates when both surface tension and mobility are anisotropic; Table IV lists some examples. A void is denoted as uncritical if it reaches a steady state (e.g., the void in Fig. 9), or collapses along the line direction. If the mobility is highly anisotropic, it controls the void evolution in a way similar to Fig. 9. If both surface tension and mobility anisotropies play roles, depending on their combinations, the critical value χ_c either increases or decreases.

VII. CONCLUDING REMARKS

Void shape change is understood in terms of surface diffusion driven by the electron wind and surface tension. In only one situation, among many that have been investigated, is the circular void stable against infinitesimal perturbation. In reality, finite imperfections exist in the interconnects. Our simulation shows that the instability is sensitive to imperfections. A void collapses into a slit if the dimensionless group $Z^*eER_0^2/\Omega\gamma$ is large.

We have described a method to simulate void shape evolution, combining a conformal mapping to determine the electric field, and the Galerkin method to construct a dynamical system of finite degrees of freedom. We could as well approximate the void perimeter by many short straight segments, and formulate a finite element procedure for the shape evolution, as has been done in Refs. 21 and 37. The resulting ordinary differential equations would look formally the same as those in Sec. V, but the finite element method

would be much more versatile. The generality of these ideas has just been appreciated.[30–35] It will be fascinating to see the ideas be implemented and applied to diverse problems in materials science in the following years.

ACKNOWLEDGMENTS

The work was supported by the NSF through Grant No. MSS-9202165, and by a grant from the Advanced Micro Devices under the supervision of Dr. J. E. Sanchez. Suo is grateful to NSF for a Young Investigator Award. Hao was supported by a visiting appointment at the University of California, Santa Barbara, funded by ONR through Contract No. N00014-93-1-0110.

[1] A. S. Oates, International Reliability Physics Symposium, tutorial manuscript, 1994 (unpublished).
[2] C. V. Thompson and J. R. Lloyd, Mater. Res. Soc. Bull., December issue, 19 (1993).
[3] J. E. Sanchez, L. T. McKnelly, and J. W. Morris, J. Appl. Phys. **72**, 3201 (1992).
[4] J. H. Rose, Appl. Phys. Lett. **61**, 2170 (1992).
[5] Y.-C. Joo and C. V. Thompson, Mater. Res. Soc. Symp. Proc. **309**, 351 (1993).
[6] M. Genut, Z. Li, C. L. Bauer, S. Mahajan, P. F. Tang, and A. G. Milnes, Appl. Phys. Lett. **58**, 2354 (1991).
[7] P. R. Besser, M. C. Madden, and P. A. Flinn, J. Appl. Phys. **72**, 3792 (1992).
[8] Shoso Shingubara and Yasushi Nakasaki, Appl. Phys. Lett. **58**, 42 (1991).
[9] O. Kraft, S. Bader, J. E. Sanchez, and E. Arzt, Mater. Res. Soc. Symp. Proc. **309**, 199 (1993).
[10] E. Arzt, O. Kraft, W. D. Nix, and J. E. Sanchez, Jr., J. Appl. Phys. **76**, 1563 (1994).
[11] J. E. Sanchez, Jr., V. Randle, O. Kraft, and E. Arzt, SPIE, J. **1805**, 222 (1992).
[12] E. Arzt and W. D. Nix, J. Mater. Res. **6**, 731 (1991).
[13] R. Kirchheim, Acta Metall. Mater. **40**, 309 (1992).
[14] M. A. Korhonen, P. Borgesen, K. N. Tu, and Che-Yu Li, J. Appl. Phys. **73**, 3790 (1993).
[15] J. R. Lloyd, J. Appl. Phys. **69**, 7601 (1991).
[16] P. S. Ho, J. Appl. Phys. **41**, 64 (1970).
[17] C.-Y. Li, P. Borgesen, and M. A. Korhonen, Appl. Phys. Lett. **61**, 411 (1992).
[18] Z. Suo, W. Wang, and M. Yang, Appl. Phys. Lett. **64**, 1944 (1994).
[19] W. Yang, W. Wang, and Z. Suo, J. Mech. Phys. Solids **42**, 897 (1994).
[20] M. Marder (unpublished).
[21] O. Kraft and E. Arzt, Appl. Phys. Lett. **66**, 2063 (1995).
[22] H. P. Longworth and C. V. Thompson, Appl. Phys. Lett. **60**, 2220 (1992).
[23] Z. Suo, Acta. Metall. Mater. **42**, 3581 (1994).
[24] D. J. Struik, *Lectures on Classical Differential Geometry*, 2nd ed. (Dover, New York, 1988).
[25] Z. Suo and W. Wang, J. Appl. Phys. **76**, 3410 (1994).
[26] C. Herring, in *The Physics of Powder Metallurgy* (McGraw-Hill, New York, 1951), p. 143.
[27] M. A. Biot, *Variational Principles in Heat Transfer* (Oxford University Press, Oxford, 1970).
[28] Q. Ma and Z. Suo, J. Appl. Phys. **74**, 5457 (1993).
[29] T.-H. Hao (unpublished).
[30] Z. Suo, Mater. Res. Soc. Symp. Proc. **338**, 379 (1994).
[31] A. Needleman and J. R. Rice, Acta Metall. **28**, 1315 (1980).
[32] J. Svoboda and I. Turek, Philos. Mag. B **64**, 749 (1991).
[33] J. Svoboda and H. Riedel, Acta Metall. Mater. **43**, 1 (1995).
[34] R. M. McMeeking and L. T. Kuhn, Acta Metall. **40**, 961 (1992).
[35] A. C. F. Cocks, Acta Metall. **42**, 2197 (1994).
[36] F. H. Wohlbier, *Diffusion and Defect Data—Solid State Data* (Trans Tech, Aedermannsdorf, Switzerlnad, 1986), Vol. 47.
[37] A. F. Bower and L. B. Freund (to be published).